Effect of Carbon Nanotube Reinforcement on the Hot Corrosion Resistance of Zirconium-Yttrium Coatings in Molten Salt

Neeluri Suresh[a*], Suraj Bhan[b]

[*a] Research Scholar, Department of Mechanical Engineering, Noida International University (NIU), GreaterNoida
[b]Assistant Professor, Department of Mechanical Engineering, Noida International University (NIU), Greater Noida,

Abstract

The present study examines the hot corrosion behavior of carbon nanotube (CNT)-reinforced zirconium-yttrium coatings on T-91 boiler tube steel in a molten salt environment consisting of Na_2SO_4–60 wt% V_2O_5 at 600 °C under cyclic conditions. The coatings were fabricated using the air plasma spray technique. Uncoated and coated specimens, along with all as-coated samples, were exposed to hot corrosion in a silicon tube furnace at 600 °C for 50 cycles. Corrosion behavior was assessed by measuring the mass gain after each cycle. The corroded products were characterized using X-ray diffraction (XRD), scanning electron microscopy (SEM), and energy dispersive X-ray analysis (EDAX).

Upon analysis, it was observed that the uncoated specimen formed a Fe_2O_3 oxide scale, which led to thermal spallation due to poor adhesion. In contrast, all the coated specimens exhibited lower mass gains, with the oxide scale adhering strongly to the substrate steel. The CNT-reinforced zirconium-yttrium coatings demonstrated superior corrosion resistance, attributed to the uniform dispersion of CNTs within the coating matrix and the formation of protective zirconium oxide in the corrosion scale.

Keywords-: Hot corrosion · Porosity · Plasma spray · CNT · T-91 steel

1. Introduction

The development of high-temperature materials is crucial for enhancing the efficiency of coal-fired thermal power plants [1–3]. To mitigate corrosion, protective coatings are applied using thermal spray techniques [4, 5]. In boilers, contaminants from fuel deposits on components lead to corrosion of the steel, causing it to fail in its intended function [4, 6]. The lifespan of these components can be extended through the use of certain ceramic coatings [7, 8]. However, thermal spray coatings often introduce porosity, which can facilitate corrosion [9, 10]. Oxides penetrate these pores, accelerating the corrosion of the base material [11].

Despite efforts to improve corrosion resistance with various coating compositions, even advanced spraying techniques cannot eliminate defects entirely [12–15]. These coatings tend to remain porous and contain microscopic cracks [16]. Corrosive chemicals can attack the base material through these defects [12, 17, 18], particularly when low-quality fuels containing sodium (Na) and vanadium (V) impurities form corrosive elements like Na_2SO_4 and V_2O_5 [19]. Consequently, there remains a pressing need to improve coating quality, reducing defects and further enhancing corrosion resistance.

This research focuses on investigating the hot corrosion behavior of air plasma-sprayed carbon nanotube (CNT)-reinforced zirconium-yttrium composite coatings on T-91 tube steel at 600 °C in a molten salt environment. T-91 was chosen as the substrate material because of its widespread use in manufacturing boiler and superheated tubes for thermal power plants. To simulate the boiler environment, Na_2SO_4–60 wt% V_2O_5 salts were used. In

actual boiler conditions, low-grade fuel leads to the deposition of condensed and molten sulfates and vanadates, which accelerate the deterioration of surface materials [20].

The kinetics of hot corrosion were analyzed through weight gain measurements after each cycle. The corroded products were thoroughly examined using X-ray diffraction (XRD) and scanning electron microscopy with energy dispersive X-ray analysis (SEM/EDAX).

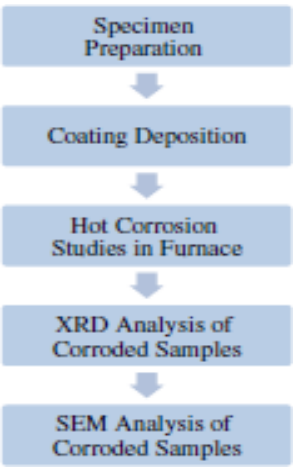

Fig. 1 Flow chart of experimental procedure

2 Experimental Procedure

2.1 Coating Preparation

Figure 1 illustrates the experimental process for studying the hot corrosion behavior of CNT-reinforced coatings on T-91 steel at 600 °C in a molten salt environment. Fresh T-91 steel tubes were sourced from the Talwandi Sabo Thermal Power Plant, Talwandi Sabo, Bathinda, Punjab (India). The specimens were sectioned from the T-91 steel tube into dimensions of 22 × 15 × 3 mm^3.

For the hot corrosion studies, zirconium yttrium (ZrO_2–Y_2O_3) powder was mixed with carbon nanotubes (CNT) in a ball mill for approximately four hours to ensure uniform distribution of the coating powders. The different CNT-reinforced coating compositions were as follows: ZrO_2–Y_2O_3–0.5 wt% CNT, ZrO_2–Y_2O_3–1 wt% CNT, ZrO_2–Y_2O_3–2 wt% CNT, ZrO_2–Y_2O_3–4 wt% CNT, and ZrO_2–Y_2O_3–6 wt% CNT. The conventional ZrO_2–Y_2O_3 coating, along with all the CNT-reinforced composite coatings, was deposited onto the T-91 steel specimens using the air plasma spray technique at Metallizing Equipment Corp. Pvt. Ltd., Jodhpur, Rajasthan (India). The coating thickness was maintained between 255 µm and 275 µm. A Minitest-2000 thin film thickness gauge was used to measure the coating thickness during the deposition process.

The porosity of the coatings was analyzed using a porosity analyzer equipped with LEICA image analysis software. The porosity of the conventional ZrO_2–Y_2O_3 coating was found to be 4.25%. As CNT was added to the ZrO_2–Y_2O_3 coating, the porosity of the composite coatings decreased. The observed porosities for the composite coatings were as follows: 3.78% for 0.5 wt% CNT, 3.62% for 1 wt% CNT, 3.52% for 2 wt% CNT, 3.45% for 4 wt% CNT, and 2.93% for 6 wt% CNT.

Table 1. Designation with composition of coatings

Designation	Chemical composition (wt.%)
S1	100%ZrO_2—Y_2O_3
S2	99.5%ZrO_2—Y_2O_3+0.5%CNT

S3	99%ZrO_2—Y_2O_3+1%CNT
S4	98%ZrO_2—Y_2O_3+2%CNT
S5	96%ZrO_2—Y_2O_3+4%CNT
S6	94%ZrO_2—Y_2O_3+6%CNT

2.2 Hot Corrosion Studies in a Molten Salt (Na2SO4–60 wt%V2O5) Environment

A silicon tube furnace was utilized to conduct hot corrosion studies at 600 °C. Prior to commencing the experiments, the physical dimensions of each specimen—length, breadth, and thickness—were measured. A minimum of five readings were taken using a digital Vernier caliper (Make: Mitutoyo, Japan), and their mean values were calculated. Initially, both uncoated and coated specimens were rinsed with acetone and subsequently dried in hot air to eliminate moisture. The specimens were then preheated in an oven at 250 °C for 2 hours.

A salt mixture consisting of Na2SO4 and 60 wt% V2O5 was prepared by mixing with distilled water and applied to the surface of the uncoated and coated specimens using a camel hair paintbrush. The salt deposition on the specimens was maintained between 3.0 to 5.0 mg cm^{-2} [21]. The coated specimens were then placed in baked alumina boats and dried in an oven at 100 °C for 3 hours to ensure the salt adhered to the specimen surfaces. Weight measurements of each specimen, along with their respective alumina boats, were recorded using a digital weighing machine.

Subsequently, the specimens with alumina boats were placed inside the silicon tube furnace for hot corrosion studies. Each hot corrosion cycle comprised 1 hour of heating in the furnace followed by a 20-minute cooling period at room temperature [22]. The weight of each specimen, including the alumina boat, was carefully measured after every cycle. Upon completing the experiments, the corroded specimens were analyzed using X-ray diffraction (XRD) and Scanning Electron Microscopy (SEM) equipped with Energy Dispersive X-ray Analysis (EDAX) to determine their elemental composition.

3 Results

3.1 Visual Observations

Uncoated and all coated T-91 specimens subjected to hot corrosion exposure at 600 °C in a molten salt environment were visually examined using a high-definition camera (Make: Canon EOS 750D, DSLR, 24.2 MP, Japan). Macrographs of the uncoated and all CNT-reinforced ZrO2–Y2O3 composite-coated T-91 specimens are presented in Fig. 2. For the uncoated specimen, as shown in Fig. 2a, scale formation was observed by the end of the third hot corrosion cycle, which persisted until the final cycle. Additionally, minor cracks appeared on the specimen's surface by the 22nd cycle, and minor spalling was evident by the 42nd cycle, continuing until the end of the exposure period.

The macrograph of the conventional ZrO2–Y2O3-coated T-91 steel specimen is shown in Fig. 2b, where a yellowish-grey coloration became apparent after the sixth hot corrosion cycle. Minor swelling of the scale on the surface was observed after the 36th cycle. Macrographs of all CNT-reinforced ZrO2–Y2O3-coated specimens are illustrated in Fig. 2c–g. These CNT-reinforced composite coatings remained intact, uniform, and crack-free throughout the hot corrosion exposure at 600 °C in the molten salt environment.

3.2 Weight Change Analysis

Figure 3 illustrates the weight gain per unit area versus time (number of cycles) for all samples subjected to hot corrosion at 600 °C in a molten salt environment. The weight gain measurements were used to analyze the kinetics of hot corrosion, where higher weight gain

by the specimens indicated a higher corrosion rate. The uncoated T-91 substrate exhibited a slight weight gain up to the 7th cycle, followed by a significant increase after the 30th cycle, as shown in Fig. 3. For the conventional ZrO2–Y2O3 coated specimen, a notable increase in weight gain was observed starting from the 25th cycle and continued until the final cycle.

All CNT-reinforced composite-coated specimens demonstrated lower weight gain throughout the hot corrosion study, as illustrated in Fig. 3. The cumulative weight gain for the conventional ZrO2–Y2O3 coated T-91 steel was recorded as 7.48 mg cm^{-2}, which is significantly lower compared to the uncoated T-91 steel specimen (38.24 mg cm^{-2}), as detailed in Table 2. This indicates that the conventional ZrO2–Y2O3 coating reduced the net weight gain by 80.43%. Furthermore, increasing the proportion of CNT in the ZrO2–Y2O3 matrix progressively decreased the overall weight gain measurements throughout the 50 cycles at 600 °C. The weight gain values for ZrO2–Y2O3 coatings with 0.5 wt%, 1 wt%, 2 wt%, 4 wt%, and 6 wt% CNT were recorded as 5.16, 3.71, 2.84, 2.01, and 1.41 mg cm^{-2}, respectively. Among all CNT-reinforced coated specimens, the ZrO2–Y2O3–6 wt% CNT coating exhibited the highest corrosion resistance, achieving a 96.31% reduction in weight gain compared to the uncoated T-91 steel specimen.

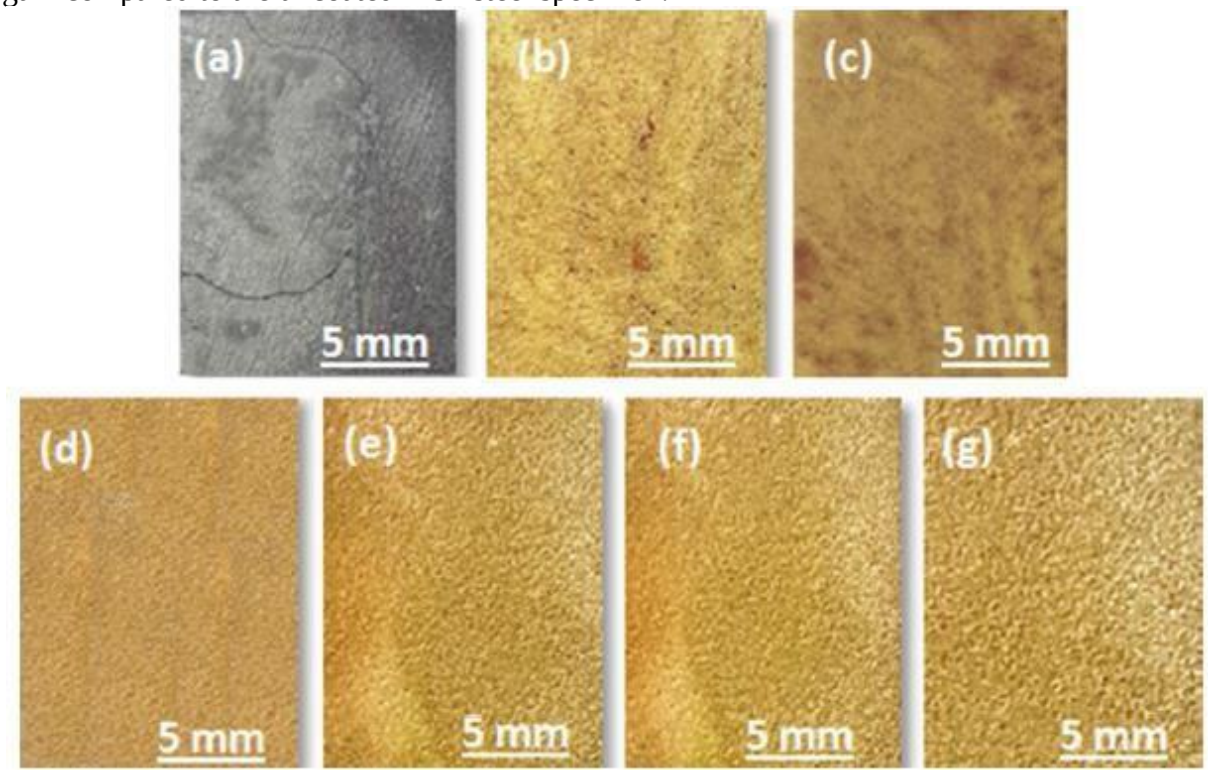

Fig. 2 Macrograph of: a Uncoated; b Conventional ZrO2–Y2O3 coated; c ZrO2–Y2O3–0.5 wt% CNT; d ZrO2–Y2O3–1wt% CNT; e ZrO2–Y2O3–2wt% CNT; f ZrO2–Y2O3–4 wt% CNT; g ZrO2–Y2O3–6 wt% CNT coated T-91 specimens after hot corrosion at 600 °C.

Figure 4 presents the (weight gain/area)² versus the number of cycles (50 cycles) for all samples after hot corrosion at 600 °C, highlighting the adherence to parabolic rate law for the coated specimens. The curve for the uncoated T-91 specimen displayed a slight deviation from the parabolic rate law, whereas the conventional ZrO2–Y2O3 coated and CNT-reinforced ZrO2–Y2O3 composite-coated T-91 specimens closely followed the parabolic rate law. The parabolic rate constant (Kp) was determined from the slope of the fitted linear

regression line. After hot corrosion exposure at 600 °C, the cumulative weight gain and the parabolic behavior of the specimens were analyzed in detail.

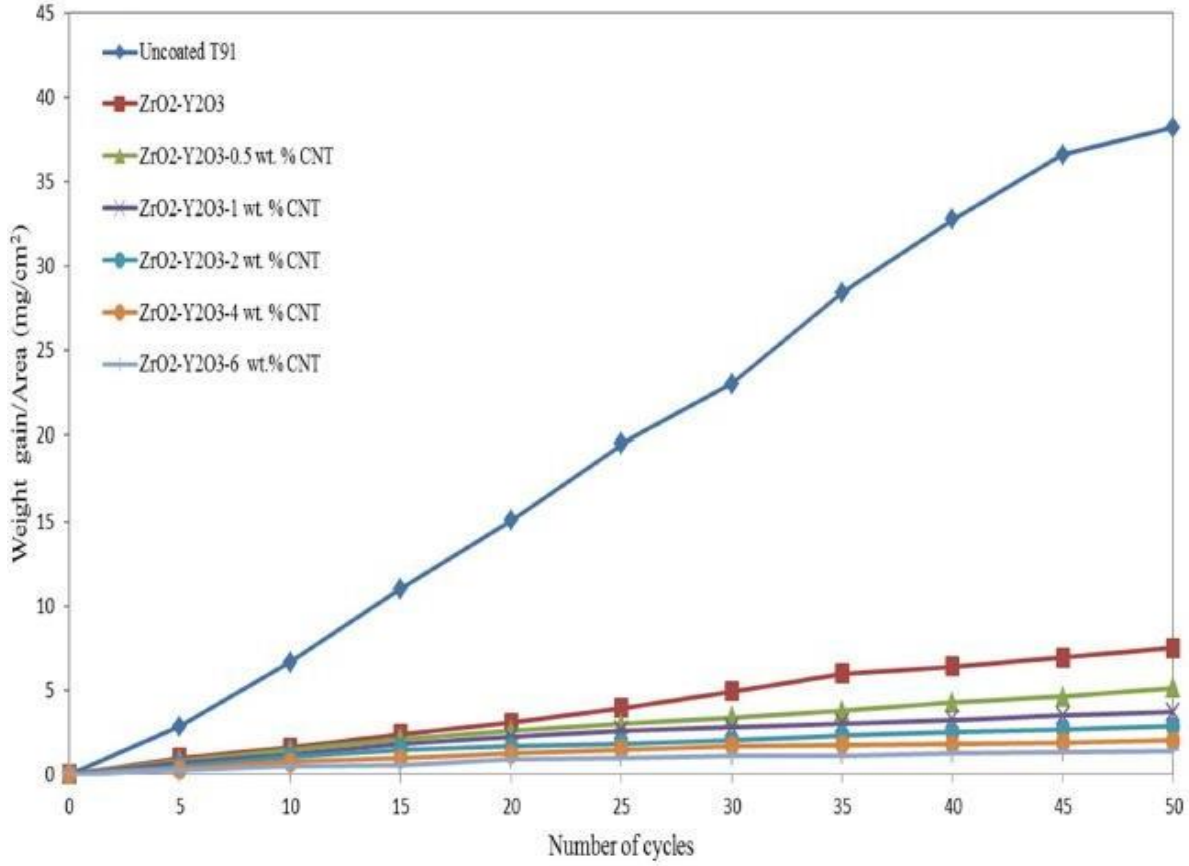

Fig. 3 Weight gain/area versus time (number of cycles) for all samples after hot corrosion at 600 °C.

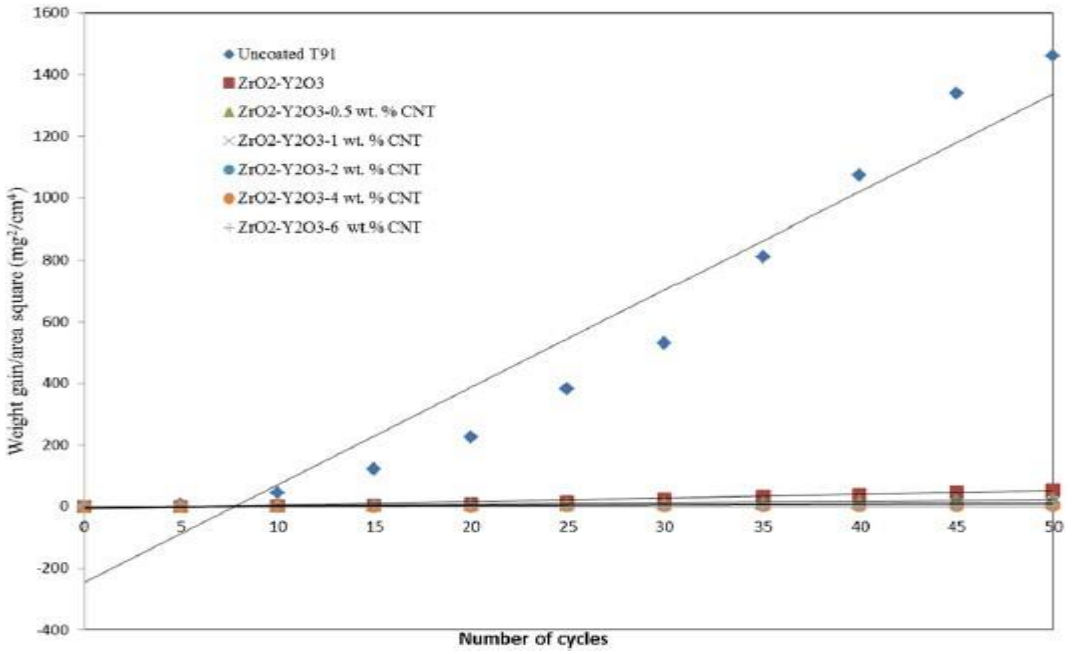

Fig. 4 (Weight gain/area)^2 versus number of cycles (50 cycles) for all samples after hot corrosion at 600 °C.

3.3 XRD Analysis

The X-ray diffraction (XRD) analysis of uncoated T-91, conventional ZrO2–Y2O3, and CNT-reinforced ZrO2–Y2O3 coated specimens after hot corrosion exposure is depicted in Fig. 6a–g. For the uncoated T-91 steel, major peaks corresponding to Fe were identified in the scale, as shown in Fig. 6a. The XRD analysis of the conventional and CNT-reinforced ZrO2–Y2O3 coated T-91 steel specimens post hot corrosion revealed ZrO2–Y2O3 (α) as the predominant phase. Additionally, minor peaks of carbon (C) were detected in all CNT-reinforced composite-coated specimens, confirming the uniform distribution of carbon nanotubes within the coating matrix.

Small spectra corresponding to Na2SO4 (n) and V2O5 (v) were also observed across all specimens, as presented in Fig. 6a–g. This confirms the formation of sulphates and vanadates during exposure to the molten salt environment at 600 °C.

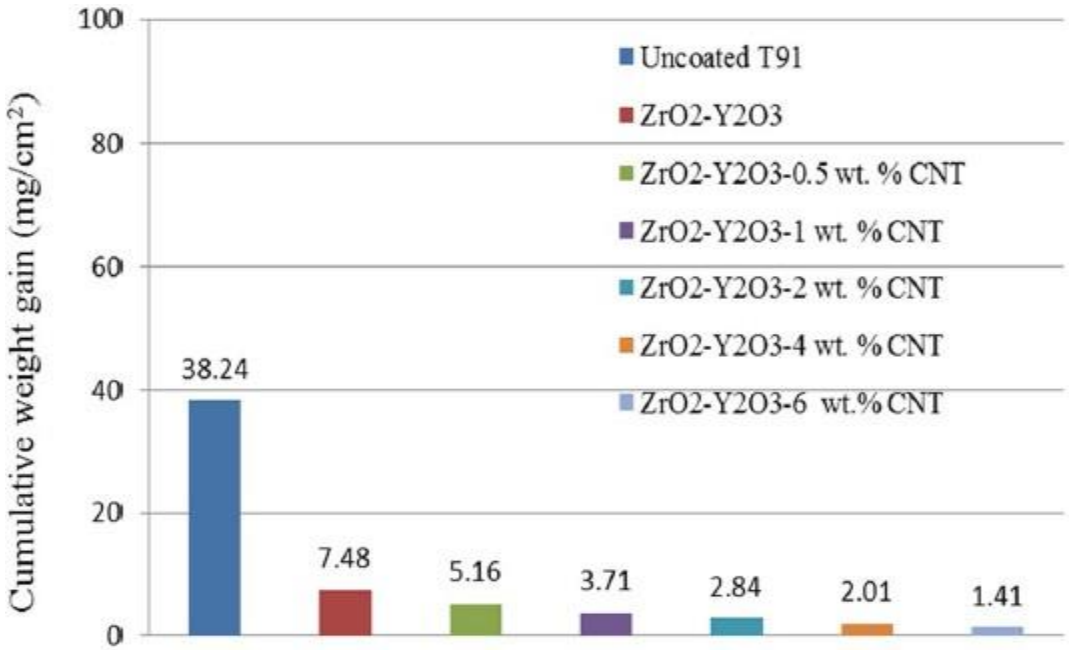

Fig. 5 Cumulative weight gain of all samples after hot corrosion at 600 °C

3.4 SEM/EDAX Analysis

FE-SEM micrographs combined with EDAX compositional analysis of uncoated, conventional ZrO2–Y2O3 coated, and all CNT-reinforced composite-coated T-91 steel specimens after hot corrosion exposure in a molten salt (Na2SO4–60 wt% V2O5) environment at 600 °C are shown in Figs. 7 and 8. The corroded oxide scale of the uncoated T-91 specimen exhibited irregularly shaped flakes with a porous structure, as depicted in Fig. 7a. EDAX analysis confirmed the oxide scale primarily consisted of Fe and O, indicating the formation of iron oxide (Fe2O3). Small amounts of Na and V were also detected in the scale composition.

The SEM micrographs of the conventional ZrO2–Y2O3 coated T-91 steel revealed a light grey and yellowish appearance (Fig. 7b). EDAX analysis at specific points indicated the

presence of Zr, Y, and O, along with minor amounts of Fe, Na, and V. The Fe likely diffused from the substrate during hot corrosion, while Na and V confirmed the presence of elements from the molten salt.

For the ZrO2–Y2O3–0.5 wt% CNT coated T-91 steel, the micrographs showed a substantial presence of Zr, Y, and O, along with minor amounts of C, Na, and V in the scale composition (Fig. 7c). The detection of C confirmed the incorporation of CNT into the coating matrix.

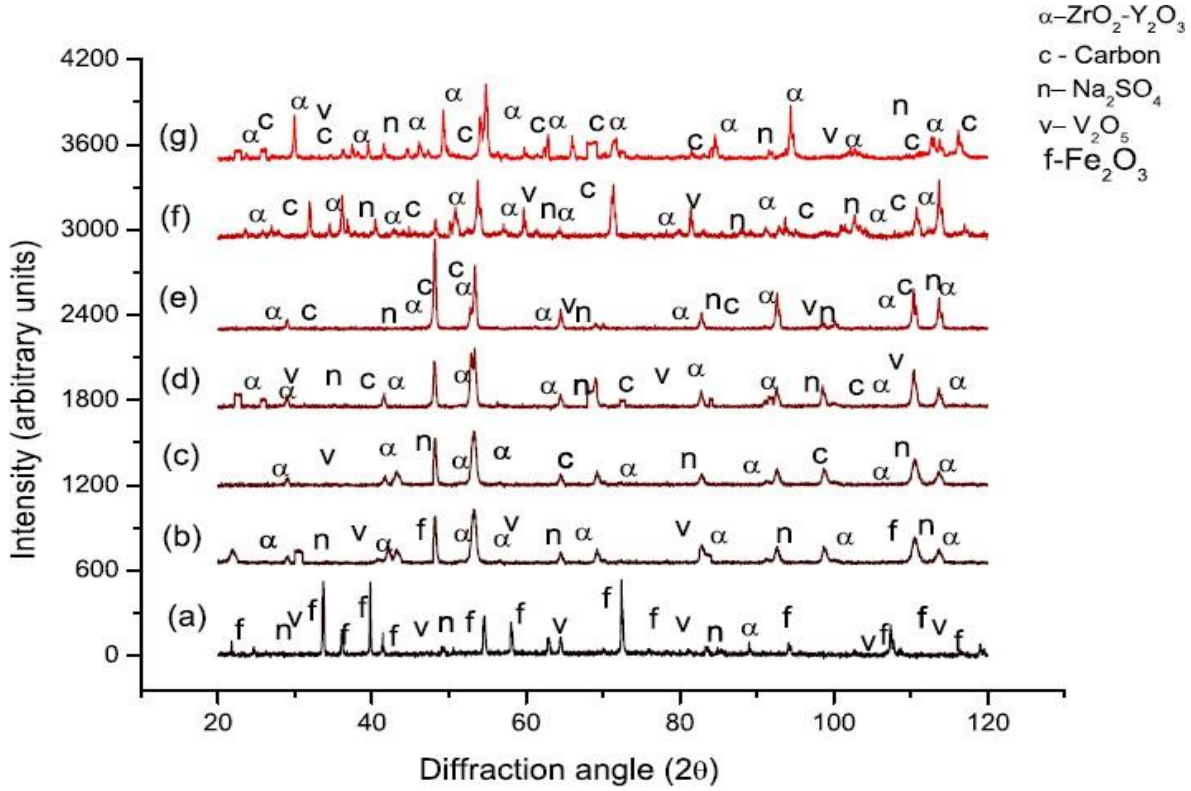

Fig. 6 XRD analysis of: a Un-coated; b Conventional ZrO2–Y2O3 coated; c ZrO2–Y2O3–0.5 wt% CNT; d ZrO2–Y2O3-1 wt% CNT; e ZrO2–Y2O3–2 wt% CNT; f ZrO2–Y2O3–4 wt% CNT; g ZrO2– Y2O3–6 wt% CNT coated T-91 steel at 600 °C.

FE-SEM micrographs with EDAX analysis for ZrO2–Y2O3 coatings reinforced with 1 wt%, 2 wt%, 4 wt%, and 6 wt% CNT are presented in Fig. 8a–d, respectively. The scale composition for all coated samples appeared intact and uniform, with a regular morphology. EDAX analysis confirmed the major constituents—zirconium, yttrium, and oxygen—across all samples. The carbon content in the scale increased proportionally with the CNT percentage in the composite coating matrix. Additionally, small proportions of Na and V were detected in all CNT-reinforced coatings, as shown in Fig. 8a–g, confirming the presence of essential elements from the molten salt after hot corrosion exposure.

4 Discussion

4.1 Coating Thickness and Porosity

The plasma spray technique was utilized to deposit the coatings on the T-91 substrate material. The coating thickness was uniformly distributed across the cross-section and maintained within the range of 255 to 270 μm, consistent with the findings of Goyal et al. [23], who developed coatings with a similar thickness range. The porosity of the conventional ZrO2–Y2O3 coating was measured at 4.25% but was significantly reduced with the

incorporation of CNT into the ZrO2–Y2O3 composite coating. This reduction in porosity was attributed to the uniform dispersion of CNT across the specimen's surface, which facilitated greater heat absorption by the powder particles, thereby enhancing the melting capacity of the coating powder.

Keshri and Agarwal [24] also reported in their research that the uniform dispersion of CNT in powder improves the melting point and enhances the heat absorption capacity, leading to a notable reduction in the coating's porosity.

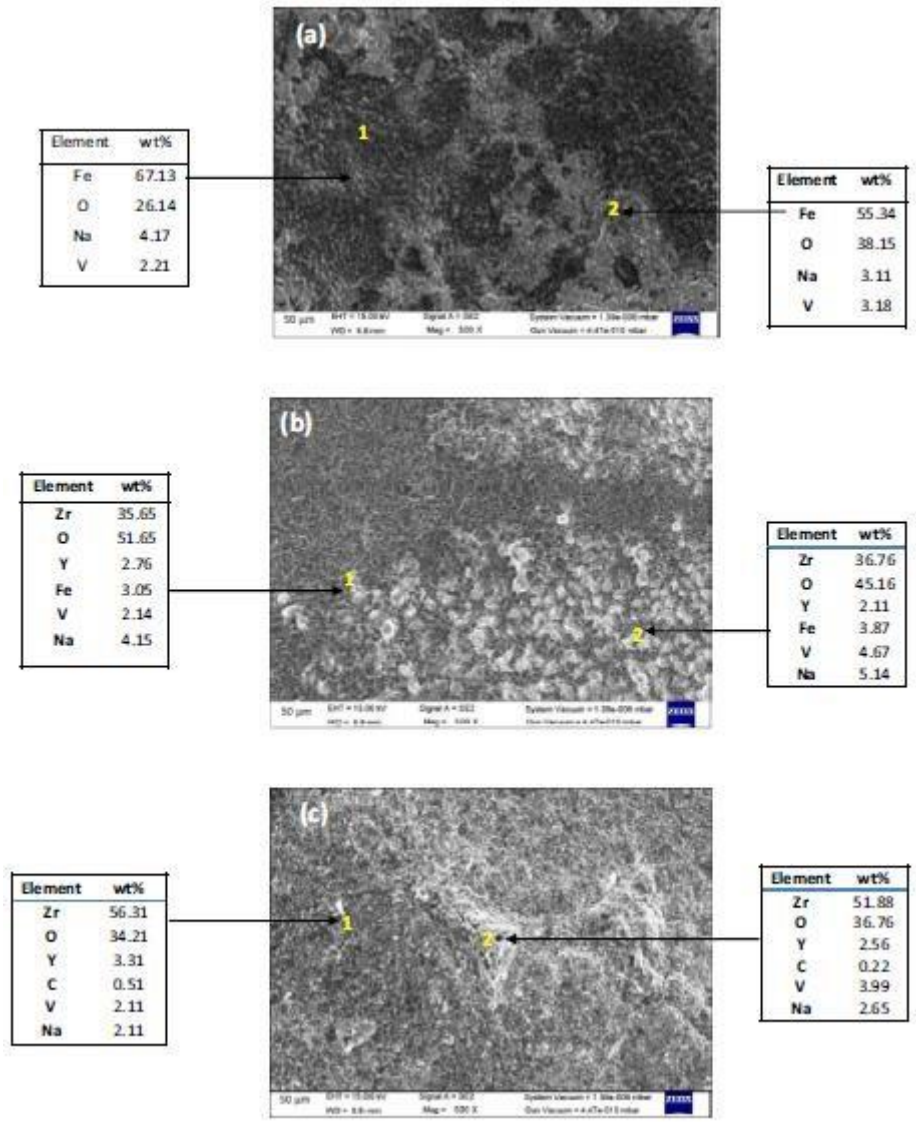

Fig. 7 SEM/EDAX analysis of: a Un-coated; b Conventional ZrO2–Y2O3; c ZrO2–Y2O3–0.5 wt% CNT coated T-91 steel specimens after hot corrosion at 600 °C.

4.2 Weight Gain Measurements

A non-protective scale of Fe2O3 was formed due to the hot corrosion of uncoated T-91 steel specimens in a molten salt environment at 600 °C during and after the complete 50 cycles. The corroded scale was observed to be thick and porous in nature, as revealed by FE-SEM and EDAX analysis. The hot corrosion study showed that the corrosion rate of uncoated T-91 steel was relatively higher in the initial stages, with the formation of an oxide scale

followed by cracks, as evident in the macrograph shown in Fig. 1. These cracks propagated during subsequent cycles, causing severe deterioration of the uncoated T-91 steel surface. For the uncoated T-91 specimen, the parabolic rate constant (Kp) was calculated as 81.238 × 10^{-10} g^2 cm^{-4} s^{-1}, and the total weight gain after 50 cycles was observed to be 38.24 mg cm^{-2}. Sidhu et al. [25] concluded that this significant weight gain was due to the formation of the non-protective Fe2O3 scale, as confirmed by XRD analysis showing the presence of Fe and O.

For the conventional ZrO2–Y2O3 coated T-91 steel, the weight gain reduction was observed to be 80.43% compared to uncoated T-91 specimens after hot corrosion at 600 °C. During the exposure, minor cracks and spallation of the scale were noted. The ZrO2–Y2O3 coating, applied using the air plasma spray technique, provided good corrosion resistance to T-91 steel. Thakare et al. [26] reported that carbon nanotubes in reinforced YSZ-alumina composite coatings act as a thermal barrier, providing excellent corrosion resistance during hot corrosion. However, Fe penetration through voids in the conventional ZrO2–Y2O3 coating caused spallation and crack formation, along with the development of a non-protective Fe2O3 scale. SEM micrographs showed a yellowish contrast phase with a lamellar structure, likely due to the oxides of zirconium and yttrium in the scale. EDAX and cross-sectional analysis identified Zr, Y, Fe, and O, along with Na and V from the molten salt used during the hot corrosion experiments.

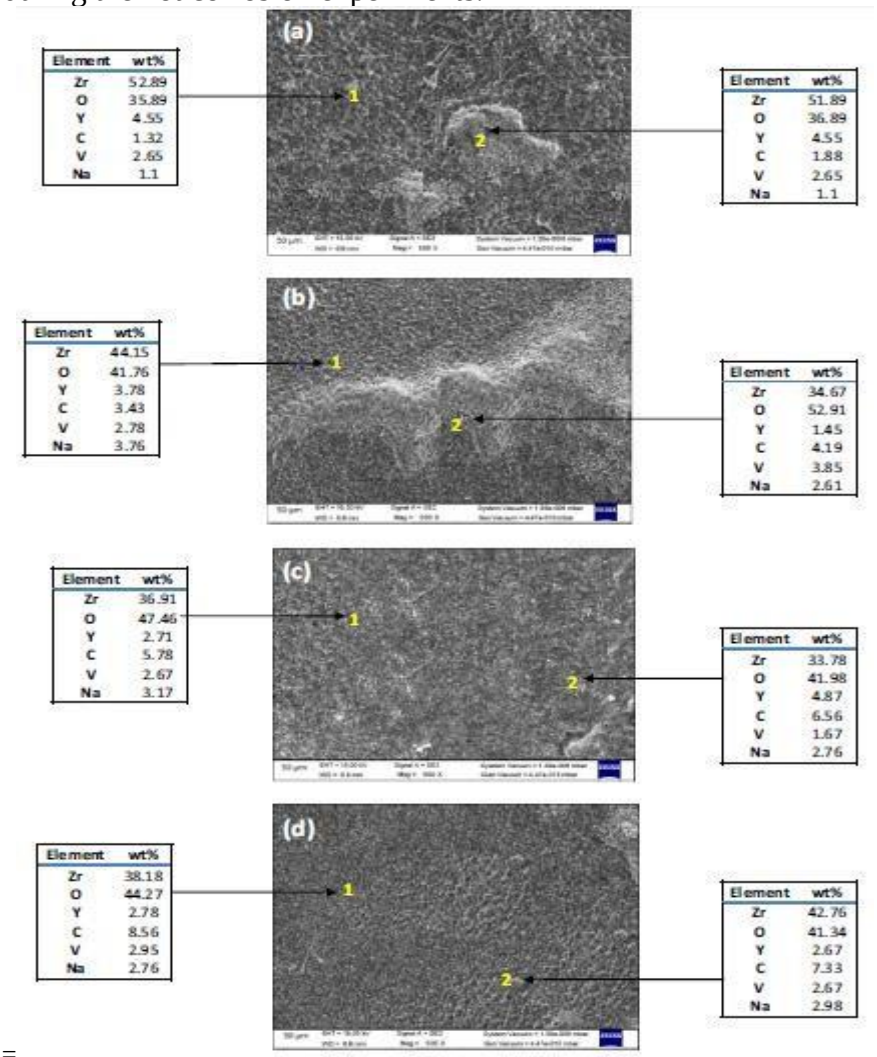

7\=

Fig. 8 SEM/EDAX analysis of: a ZrO2–Y2O3–1 wt% CNT; b ZrO2–Y2O3–2 wt% CNT; c ZrO2–Y2O3–4 wt% CNT; d ZrO2– Y2O3–6 wt% CNT coated T-91 steel specimens after hot corrosion at 600 °C.

In CNT-reinforced ZrO2–Y2O3 composite coatings, weight gain plots indicated effective protection of the T-91 substrate steel from hot corrosion at 600 °C. After 50 cycles, the specimens remained crack-free and intact, with no spallation. Prasanna et al. [27] demonstrated that the formation of NiCr2O4 and Ni2O3 oxides provides superior corrosion resistance in coated substrates compared to bare substrates in molten salt environments under high-temperature conditions. The cumulative weight gain was significantly reduced by the addition of CNT to the coating matrix, with the lowest weight gain recorded for ZrO2–Y2O3–6 wt% CNT coated T-91 steel (1.41 mg cm^{-2}), making it the most resistant to hot corrosion among all specimens exposed at 600 °C in the molten salt environment. Sharma et al. [28] studied Ni–Cr–Ti and Ni–5Al coatings on T-91 and T-22 steel and reported that coated specimens exhibited better corrosion resistance than bare substrates. T-91 coated specimens provided superior oxidation resistance, as evident from weight change analysis, compared to T-22 specimens, due to their higher hardness and the protective chromium oxide layer on the coated surface.

4.3 Structural and Elemental Comparison

In the XRD analysis of all the as-coated T-91 steel specimens, ZrO2–Y2O3 emerged as the predominant phase, with minor peaks of carbon attributable to the inclusion of CNT in the composite coating matrix. Ahmad et al. [28] and Goyal et al. [21] similarly reported carbon peaks in their XRD spectra, confirming uniform reinforcement within the coating matrix. The formation of a protective oxide layer of ZrO2–Y2O3 in all CNT-reinforced coated specimens significantly enhanced resistance to hot corrosion. Gond et al. [29] concluded in their studies that T-91 steel exhibited superior corrosion resistance compared to T-22 steel, potentially due to the absence of an NiO layer in the scale after hot corrosion studies under elevated temperatures in similar environments. SEM/EDAX analysis at selected points verified the presence of Zr, Y, O, and C elements, with a consistent distribution of CNT across the specimen surfaces. This uniform distribution of CNT contributed to reduced coating porosity, thereby impeding the penetration of corrosive elements into the substrate. Meng et al. [30] observed that CNT effectively filled the pores in the coating, further reducing porosity. The reinforcement of CNT in the ZrO2–Y2O3 coating created a dense structure, enhancing the corrosion resistance of the conventional ZrO2–Y2O3 coating.

5 Conclusion

The current study investigated the hot corrosion behavior of CNT–ZrO2–Y2O3 reinforced coatings on T-91 steel at 600 °C in a molten salt environment, leading to the following conclusions:

1. The uncoated T-91 steel demonstrated significant mass gain and a higher corrosion rate, leading to the formation of a thick, porous, and nonprotective Fe2O3 scale during hot corrosion studies in a molten salt environment at 600 °C.
2. For conventional ZrO2–Y2O3 coated T-91 steel, the weight gain was reduced by 80.43% compared to uncoated T-91 specimens after hot corrosion at 600 °C. However, minor cracks and scale spallation were observed during exposure.
3. All CNT-reinforced ZrO2–Y2O3 coated T-91 steel specimens exhibited significantly lower weight gain compared to uncoated and conventionally coated T-91 specimens. Additionally, the coatings remained intact, crack-free, and showed no spallation during the investigations.
4. XRD analysis of all CNT-reinforced coatings identified ZrO2 and Y2O3 as the

primary phases and carbon as a minor phase. The presence of these elements was further confirmed by EDAX analysis.

5. The incorporation of CNTs reduced porosity by filling voids within the coating matrix, thereby enhancing the hot corrosion resistance of ZrO2–Y2O3 coatings on boiler steels.

References

1. Duarte CA, Espejo E, Martinez JC (2017) Failure analysis of the wall tubes of a water-tube boiler. Eng Fail Anal 79(January): 704–713. https ://doi.org/10.1016/j.engfa ilana l.2017.05.032
2. Alia FF et al (2017) High temperature oxidation in boiler environment of chromized steel. IOP Conf Ser. https ://doi.org/10.1088/1757-899X/257/1/01208 6.
3. Kumar D, Pandey KN, Das DK (2016) Microstructure studies of air-plasma-spray-deposited CoNiCrAlY coatings before and after thermal cyclic loading for high-temperature application. Int J Miner Metall Mater 23(8):934–942. https ://doi.org/10.1007/s12613-016-1309-x
4. Ding Q, Tang X, Yang Z (2017) Failure analysis on abnormal corrosion of economizer tubes in a waste heat boiler. Eng Fail Anal 73:129–138. https ://doi.org/10.1016/j.engfa ilana l.2016.12.011
5. Keyvani A, Bahamirian M (2016) Oxidation resistance of Al2O3 - nanostructured/CSZ composite compared to conventional CSZ and YSZ thermal barrier coatings. Mater Res Express 3(10):1–12
6. Loghman-estarki MR, Nejati M, Edris H, Shoja R (2016) Comparison of hot corrosion behavior of nanostructured ScYSZ and YSZ thermal barrier coatings in the presence of molten sulphate and vanadate salt Evaluation of hot corrosion behavior of plasma sprayed scandia and yttria co-stabilized nanostructured therma. J Eur Ceram Soc 35(2):693–702. https ://doi.org/10.1016/j.jeurc erams oc.2014.08.029
7. Goyal K, Goyal R (2019) Improving hot corrosion resistance of Cr3C2–20NiCr coatings with CNT reinforcements. Surf Eng. https ://doi.org/10.1080/02670 844.2019.16626 45
8. Jiang C, Xing Y, Zhang F, Hao J (2012) Microstructure and corrosion resistance of Fe/Mo composite amorphous coatings prepared by air plasma spraying. Int J Miner Metall Mater 19(7):657–662. https ://doi.org/10.1007/s1261 3-012-0609-z
9. Saladi S, Menghani J, Prakash S (2014) Hot corrosion behaviour of detonation-gun sprayed Cr3C2– NiCr coating on Inconel-718 in molten salt environment at 900 °C. Trans Indian Inst Metals 67:623–627. https ://doi.org/10.1007/s1266 6-014-0383-x
10. Huang L, Meng H, Liang L, Li S, Shi J (2015) Effects of heat treatment on the corrosion resistance of carbon steel coated with LaMgAl11O19 thermal barrier coatings. Int J Miner Metall Mater 22(10):1050–1059. https ://doi.org/10.1007/s1261 3-015-1167-y
11. Pal V, Sidhu S, Goyal K (2017) Comparative study of corrosion behaviour of HVOF-coated boiler steel in actual boiler environment of a thermal power plant. J Austral Ceram Soc. https ://doi.org/10.1007/s4177 9-017-0107-x
12. Bengtsson P, Johannesson T (1995) Characterization of microstructural defects in plasma-sprayed thermal barrier coatings. J Therm Spray Technol 4(3):245–251. https ://doi.org/10.1007/ BF026 46967
13. Fargas G, Casellas D, Llanes L, Anglada M (2003) Thermal shock resistance of yttria-stabilized zirconia with Palmqvist indentation cracks. J Eur Ceram Soc 23(1):107–114. https ://doi.org/10.1016/ S0955 -2219(02)00065 -1
14. Saremi M, Afrasiabi A, Kobayashi A (2007) Bond coat oxidation and hot corrosion

behavior of plasma sprayed YSZ coating on Ni superalloy. Trans JWRI. 36(1):41–45
15. Tianshun D, Xiukai Z, Guolu L, Li L, Ran W (2018) Microstructure and corrosive wear resistance of plasma sprayed Ni-based coatings after TIG remelting. Mater Res Express 5(2):026411

16. Fukanuma H (1994) A porosity formation and flattening model of an impinging molten particle in thermal spray coatings. J Thermal Spray Technol 3(1):33–44
17. Chatha SS, Sidhu HS, Sidhu BS (2012) Characterisation and corrosion-erosion behaviour of carbide based thermal spray coatings. J Miner Mater Charact Eng 11(06):569–586. https :// doi.org/10.4236/jmmce .2012.11604 1
18. Kamal S, Jayaganthan R, Prakash S (2009) Evaluation of cyclic hot corrosion behaviour of detonation gun sprayed Cr3C2- 25%NiCr coatings on nickel- and iron-based superalloys. Surf Coatings Technol 203(8):1004–1013. https ://doi.org/10.1016/j.surfc oat.2008.09.031
19. Sapundjiev D, Van Dyck S, Bogaerts W (2006) Liquid metal corrosion of T91 and A316L materials in Pb–Bi eutectic at temperatures 400–600 °C. Corrosion Sci 48(3):577–594. https ://doi.org/10.1016/j.corsc i.2005.04.001
20. Goyal R, Sidhu BS, Chawla V (2018) Oxidation behaviour of plasma sprayed carbon nanotubes-alumina coated ASME-SA213-T291 boiler tube steel. J Mater Metall Eng 7(3):1–15
21. Goyal K, Singh H, Bhatia R (2019) Hot-corrosion behavior of Cr2O3- CNT-coated ASTM-SA213-T22 steel in a molten salt environment at 700 °C. Int J Miner Metall Mater 26(3):337–344
22. Singh S, Goyal K, Goyal R (2016) Performance of Cr3C2-25 (Ni20Cr) and Ni–20Cr coatings on T22 boiler tube steel in simulated boiler environment. J Thin Films Coat Sci Technol Appl 3(2):19–26
23. Goyal K, Singh H, Bhatia R (2019) Hot-corrosion behavior of Cr2O3-CNT-coated ASTM-SA213-T22 steel in a molten salt environment at 700°C. Int J Miner Metall Mater 26(3):337–344. https://doi.org/10.1007/s1261 3-019-1742-8
24. Keshri AK, Agarwal A (2011) Splat morphology of plasma sprayed aluminum oxide reinforced with carbon nanotubes: a comparison between experiments and simulation. Surf Coatings Technol 206(2–3):338–347. https ://doi.org/10.1016/j.surfcoat.2011.07.025
25. Sidhu VPS, Goyal K, Goyal R (2017) Comparative study of corrosion behaviour of HVOF-coated boiler steel in actual boiler environment of a thermal power plant. J Aust Ceram Soc 53(2):925–932. https ://doi.org/10.1007/s4177 9-017-0107-x
26. Thakare JG, Pandey C, Mulik RS, Mahapatra MM (2018) Mechanical property evaluation of carbon nanotubes reinforced plasma sprayed YSZ-alumina composite coating. Ceram Int44(6):6980–6989
27. Prasanna PA, Sreenivasulu PSV (2018) High-temperature corrosion behaviour of HVOF sprayed Cr3C2– 25NiCr coated on alloy X22CrMoV12–1 at 600 °C. J Therm Spray Eng 1(1):7–12
28. Sharma V, Kumar S, Kumar M, Deepak D (2019) High temperature oxidation performance of Ni-Cr-Ti and Ni-5Al coatings. Mater Today Proc. https ://doi.org/10.1016/j.matpr .2019.11.048
29. Gond D et al (2010) Oxidation studies of T-91 and T-22 boiler steels in air at 900 °C. J Miner Mater Charac Eng 9(8):749–761
30. Meng X, Tan X, Meng B, Yang N, Ma ZF (2008) Preparation and characterization of yttria-stabilized zirconia nanotubes. Mater Chem Phys 111(2–3):275–278. https ://doi.org/10.1016/j.match emphy s.2008.04.017